Oxidation of Metals, Vol. 15, Nos. 5/6, 1981

Effect of Ti and Ta on the Oxidation of a Complex Superalloy

Sherwin W. Yang*

Received February 4, 1980

The oxidation behaviors of a series of directionally solidified Ni-base superalloys were studied at 1000 and 1100°C. These alloys are based on a composition of Ni–4.2Co–4.8Cr–12.8Al–1.6W3.1Mo–1.0Re (at.%), with additions of Ta and Ti. Both Ta and Ti partition to alloy phases in a manner similar to Al. With addition of 1 at.% of Ta, the oxidation resistance is improved significantly, while 1 at.% of Ti appears to have no effect. Raising the concentration of Ta and Ti to 3 at.% degrades the oxidation resistance. the degradation is especially severe with 3 at.% of Ta. At only 1 at.% of Ta and Ti, both alloys establish a protective layer of Al_2O_3. The loss of the oxidation resistance at 3 at.% addition of Ta and Ti is related to the formation of complex oxides which are less protective. Detailed analysis of the oxide phases are conducted using a combination of X-ray diffraction and SEM. Characterizations of the oxidation behaviors are made under isothermal and cyclic conditions. The discrepancies between data obtained under both conditions were noted.

KEY WORDS: oxidation; superalloy; high temperature.

INTRODUCTION

The demand for improved efficiency of gas turbines requires materials that can be operated at temperatures exceeding 1100°C. Nickel–base superalloys are the primary blade and vane materials used in gas turbines. The understanding of the high-temperature oxidation behavior of complex superalloys is vital for development of new alloys.

*General Electric Company, Corporate Research & Development Center, Schenectady, New York 12301.

0030-770X/81/0600-0375$03.00/0

The Ni-base alloys normally derive their oxidation resistance by forming a protective layer of Cr_2O_3 or Al_2O_3. Fundamental studies of the oxidation of the Ni-base alloys are, therefore, often made on the simple binary systems such as Ni-Al,[1] Ni-Cr,[2] or the ternary system of Ni-Cr-Al.[3] The roles of alloying elements other than Cr and Al are rarely addressed. Previous work on the oxidation of commercial superalloys[4,5] emphasized alloys of high Cr content. However, the quest for high-temperature strength in superalloys has lead to a trend in superalloy compositions of increased Al and reduced Cr contents. More information on the oxidation of the high Al-low Cr alloys appears to be desirable.

Previous work in this laboratory revealed that the addition of Ti and Ta has an unusually beneficial effect on the cyclic oxidation behavior of the complex superalloy Ni-4.2Co-4.8Cr-12.8Al-1.6W-3.1Mo-1.0Re (at.%).[6] In reviewing the oxidation of complex superalloys, Wallwork[7] has pointed out the need to identify the effect of Ti on the oxidation of superalloys. In his examples, Udiment 700 (15.94Cr, 8.71Al, 17.35Co, 3.0Mo, 4.04Ti, 0.69C, balance Ni, at.%) forms a protective scale of Al_2O_3 upon oxidation, while IN-100 (19.56Cr, 10.91Al, 13.63Co, 1.67Mo, 5.25Ti, 0.80C, 1.05V, 0.04Zr, 0.07B, balance Ni, at.%) produces NiO and TiO_2 with Al oxidized internally.

In Ni-base superalloys, both Ti and Ta partition to the γ' phase, and both are strong formers of monocarbide.[5] Therefore, replacing Ti with Ta, in equal atomic percent, should not significantly alter Cr and Al concentrations in γ and γ' phases. Since both elements have been used as alloying additions to superalloys, largely for strengthening purpose, it is of interest to investigate the effect of these two elements on the oxidation resistance.

This present research examines the effect of Ta and Ti separately in a directionally solidified superalloy based on Ni-4.2Co-4.8Cr-12.8Al01.6W-3.1Mo-1.0Re (at.%). Characterization of the oxidation kinetics were made using a thermogravimetric technique (TGA), and the spalling behavior of the oxide was evaluated with cyclic oxidation tests. X-ray diffraction and SEM-EDAX techniques were also used for further examination.

EXPERIMENTAL PROCEDURES

Specimen Preparation

The nominal compositions of the alloys under study are in Table I. The materials were melted under an argon atmosphere in MgO crucibles. These alloys were directionally solidified as 2.2-cm (0.875 in.)-diameter cylinders at a rate of 38 cm/hr (15 in./hr) in recrystallized alumina tubes.

Table I. Nominal Composition of the Alloys Under Study[a]

	Ni	Co	Cr	Al	W	Mo	Re	Ta	Ti
Base	71.3	4.2	4.8	12.8	1.6	3.1	1.0		
A	71.5	4.2	4.8	12.8	1.6	3.1	1.0	1.0	
B	69.5	4.2	4.8	12.8	1.6	3.1	1.0	3.0	
C	71.5	4.2	4.8	12.8	1.6	3.1	1.0		1.0
D	69.5	4.2	4.8	12.8	1.6	3.1	1.0		3.0

[a]at.%.

A section 1.3 cm (0.5 in.) long was taken from the ingot starting at about 0.63 cm (0.25 in.) from the bottom of the directionally solidified region. This was cut into oxidation coupons for the thermogravimetric analysis. The coupons were approximately 1 cm × 0.5 cm × 0.15 cm (0.4 in. × 0.2 in. × 0.06 in.) with the longest edge being parallel to the growth direction. An 0.08-cm (1/32-in.)-diameter hole was drilled in each coupon for support during oxidation. The coupons were polished with 1 μ Al_2O_3.

A 3.8-cm (1.5-in.) long section was taken from each ingot at a position immediately above the region machined for coupons. Pins of 0.25-cm (0.1-in.) diameter were taken from this section by EDM and grinding. Cyclic oxidation tests were conducted using these pins in the as-ground condition.

Isothermal and Cyclic Oxidation

Isothermal oxidation tests were conducted at 1000 and 1100°C. Cyclic oxidation tests were conducted at 1100°C. The isothermal oxidation kinetics were determined by continuous measurement of weight change using a Cahn RG-electrobalance. The experimental setup is shown schematically in Fig. 1. The oxidation coupon was suspended from the balance with a 0.013-cm (0.005-in) Pt–10% RH wire which ran through a water circulating condenser with 0.7-cm I.D. The oxidizing atmosphere used was compressed air dried with drierite columns. The flow rate was 1.6 cm^3/sec (0.2 ft^3/hr) (STP). The funace was heated to a predetermined temperature before it was raised up and around the specimen. The temperature was measured by a thermocouple inserted inside the quartz oxidation tube. A six-stage radiation shield was used inside the tube to cut down air convection and thermal fluctuation.

During isothermal oxidation tests, the weight change information was recorded every 2 min in the first 2 hr of the oxidation run. The recording interval was lengthened to 5 min in the next 15 hr and it was further lengthened to 20 min or 30 min thereafter depending on the rate of weight change. In each instance of data recording, the voltage (representing the

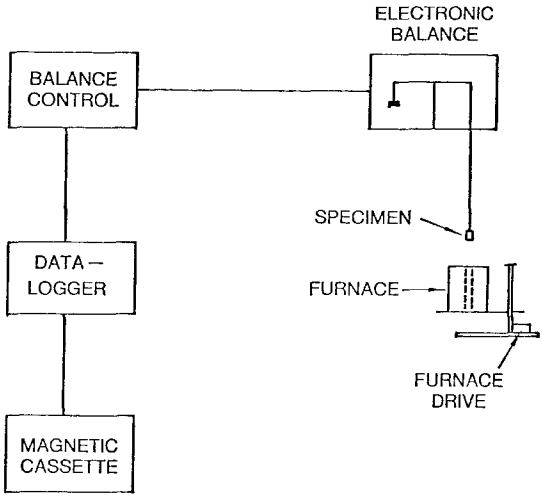

Fig. 1. Schematics of the experimental setup for studying the kinetics of isothermal oxidation.

weight), the temperature and the time of recording were digitized through a datalogger and were stored in a magnetic cassette for subsequent analysis. A regression analysis was performed on curves representing weight change vs. time. Each oxidation run typically lasted for a period of two to three days. The typical scatter of the data, after converting to mg/cm^2, amounted to $+0.06\ mg/cm^2$.

The cyclic oxidation was performed by positioning the specimen in and out of a furnace already at 1100°C. The cycle used was 50 min in and 10 min out. The weight was checked at a somewhat arbitrary interval based on the weight changes already observed.

The specimens oxidized in either test were examined by light microscopy, scanning electron microscopy, and EDAX analysis. The structures of the oxides were also examined by scraping the scales off selected specimens using Debye–Scherrer technique.

RESULTS

The microstructures of the alloys are shown in Fig. 2. The microstructures consist of fine γ' particles evenly distributed in the γ matrix. For the case of alloy D (3 at.% Ti) a coarse interdendritic γ' is also present.

Isothermal Oxidation

The isothermal oxidation results are shown in Fig. 3 for 1000°C and Fig. 4 for 1100°C. All alloys show an initially rapid weight change followed by an

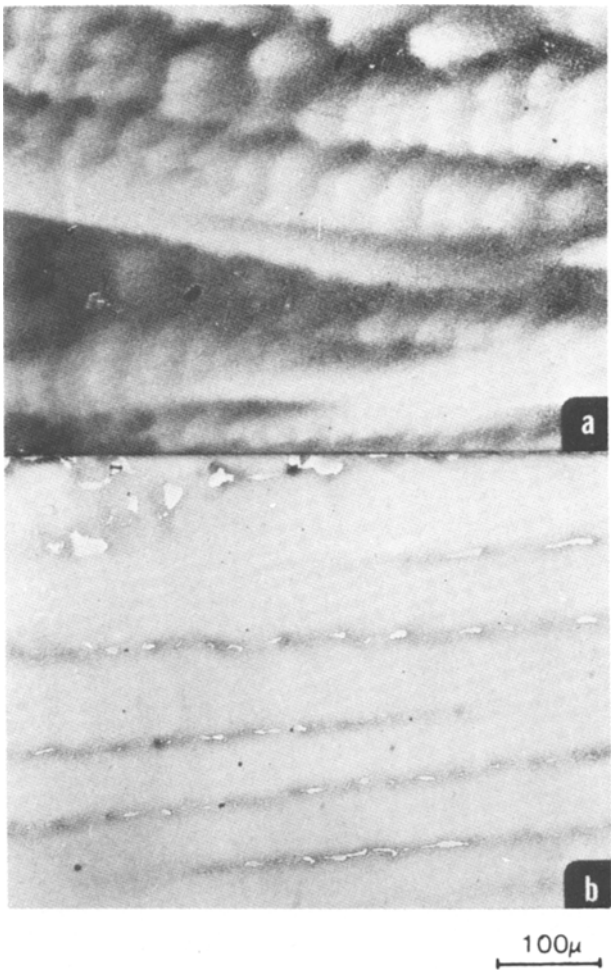

Fig. 2. Microstructure of alloys studied: (a) microstructure of alloy C (similar structures are also observed in alloys A and B); (b) microstructure of alloy D.

extended period of slow weight change. In most instances, the overall weight change in 1100°C oxidation was higher than that in 1000°C oxidation. Alloy D (3 at.% Ti) is an exception with a higher weight gain at 1000°C.

The scale spallations were checked by examining a quartz collection basket located under the oxidation coupons after each isothermal oxidation test. For alloy A, no spallation was observed after oxidation at both temperatures. Slight spallation was seen for alloys B and D at both temperatures. In order to assess whether the spallation occurred during

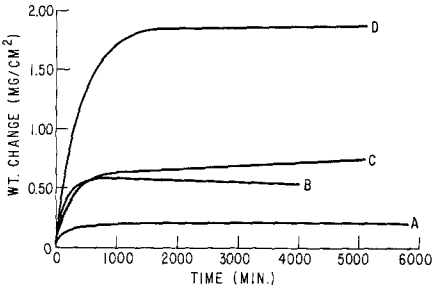

Fig. 3. 1000°C isothermal weight gain.

isothermal oxidation or during the cooling, a specimen of each alloy was attached to an alumina rod. The specimen was then inserted into the hot zone of a horizontal furnace with a collection crucible already in place. After a designated amount of time, the specimen was withdrawn from the hot zone, and the crucible was subsequently removed for examination. In this fashion, the specimen underwent cooling away from the collecting crucible, and the spall collected was representative of that which occurred during isothermal oxidation. This examination was made for 12 hr of oxidation at 1100°C and for 24 hr of oxidation at 1000°C. The results showed that isothermal spallation occurred for alloys B and D at 1100°C. At 1000°C, only alloy B showed spallation in 24 hr. These spalling observations reveal that the kinetic curves of oxidation for alloy B at 1000°C was misleading due to the isothermal spalling. Similarly, at 1100°C, the oxidation of alloys B and D is greater than that shown in Fig. 4.

The typical surface morphology after the isothermal oxidation is shown in Fig. 5. It is seen that a layer of well-defined oxide crystals is covering the outside surface. This layer is rather fragile and, in some places could be removed by a cotton swab.

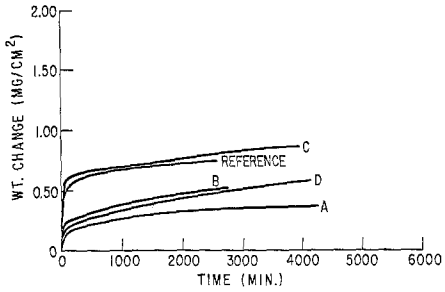

Fig. 4. 1100°C isothermal weight gain.

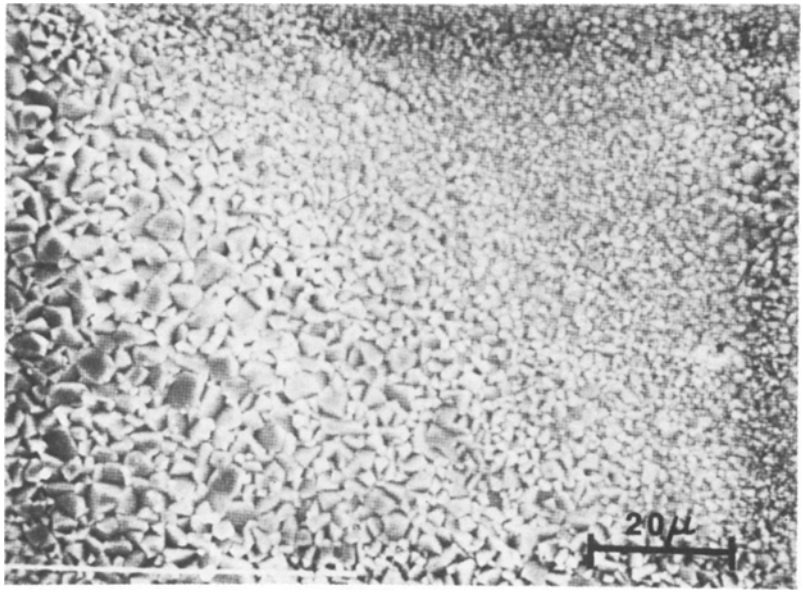

Fig. 5. Surface morphology of alloy C after isothermal oxidation at 1100°C for 24 hr.

By polishing through the cross section of the oxidized specimens, it is found that the scales usually consisted of duplex oxides. The outer scale was often lost during the specimen mounting processes. The microstructures of the specimens are shown in Figs. 6 and 7. In each case, a layer of γ'-denuded zone is found underneath the oxide layer. The denudation zone recesses further into the base metal near the grain boundaries, indicating a faster outward diffusion of Al in the boundaries.

Oxide Phase Identification

The oxides present after isothermal oxidation were identified using Debye–Scherrer technique and are listed in Table II. SEM observations were made on specimens oxidized at 1100°C for 60 hr. The oxidized specimens were intentionally scratched using a pointed steel scriber. Typically, as in the case of alloy A, two layers of oxides can be observed, which are shown in Fig. 8. The energy dispersive X-ray spectrum of the outer layer indicates the presence of Ni and Cr, but differs from the substrate metal (identified as area 2) by having lower refractory element and aluminum content. The tungsten peak in the spectrum can actually include Ta and Re

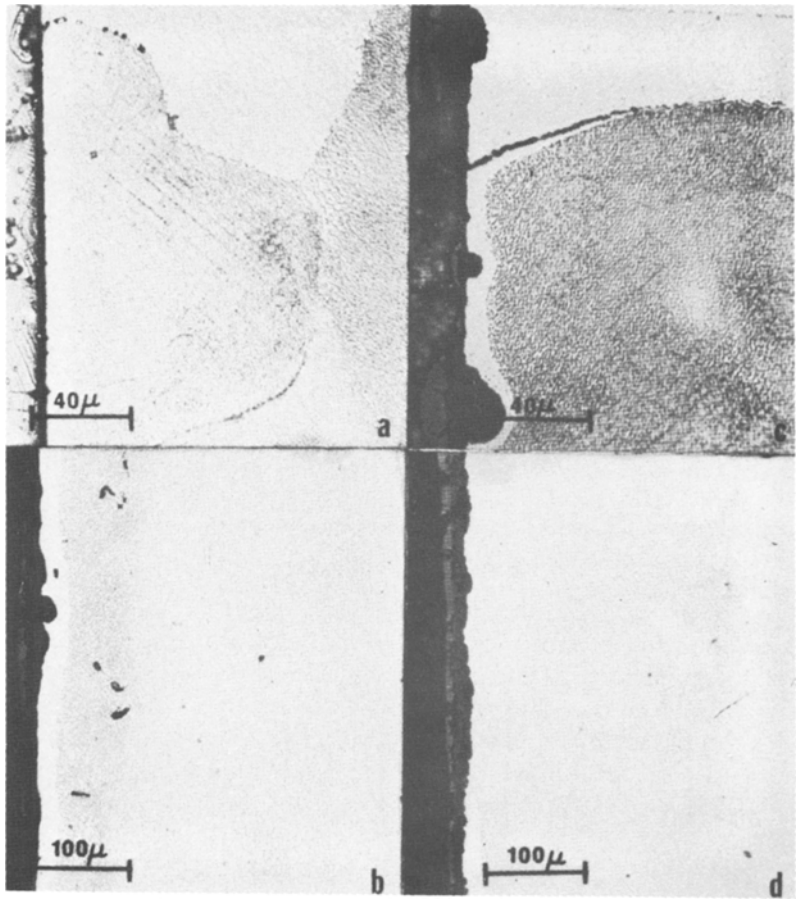

Fig. 6. (a)–(d) Microstructures of cross sections of specimens oxidized at 1000°C. (a) alloy A, (b) alloy B, (c) alloy C, (d) alloy D.

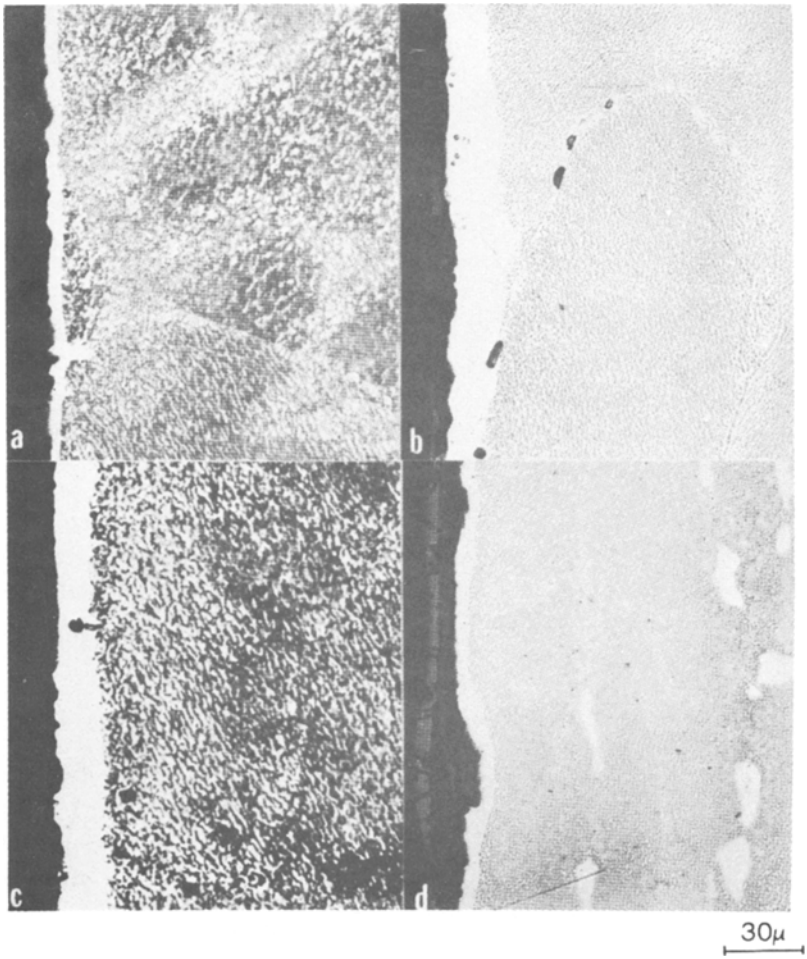

Fig. 7. (a)–(d) Microstructures of cross sections of specimens oxidized at 1100°C. (a) alloy A, (b) alloy B, (c) alloy C, (d) alloy D.

Table II. Oxides Present After Isothermal Oxidation

	Alloy			
Temp./time	A	B	C	D
1000°C/70 hr	Al_2O_3 Cr_2O_3 NiO	NiO $NiMoO_4$ $NiTa_2O_6$	$NiMoO_4$ NiO Al_2O_3 Spinel[a]	NiO $MMoO_4$ MWO_4
1100°C/1.5 hr	NiO $NiTa_2O_6$	NiO $NiTa_2O_6$	NiO $NiTiO_3$	NiO $NiTiO_3$
1100°C/60 hr	Al_2O_3 NiO Spinel[a]	NiO TaO_2 MAl_2O_4 M_2CrO_4	Al_2O_3 NiO Spinel[a]	NiO MAl_2O_4 M_2CrO_4 $NiTiO_3$*

[a]Trace.

peaks which are difficult to resolve using the standard solid state detector. The inner layer of oxide (identified as area 3) contains much more Al than the outer layer. In light of the results from X-ray diffraction, the outer Ni-rich layer is the NiO phase; and the inner layer is Al_2O_3.

The distributions of the more important alloying elements were determined qualitatively with X-ray mapping. These are shown in Figs. 9–12 for specimens oxidized at 1100°C. It is clear that these alloys form multiple layers of oxide with the outermost layer being NiO. Beneath the NiO layer, Cr, and Al are noticeably enriched. However, as shown in Table II, a protective layer of Al_2O_3 is not established in alloys B and D. Addition of high concentrations of Ta or Ti appears to have altered the stability of Al_2O_3 in favor of the complex oxides identified by X-ray diffraction. Although not shown here, areas of internal oxidation were found in alloy B. X-ray mapping showed that these areas were covered by an oxide layer enriched in Ta, W, Re, and Cr; followed by an Al-rich layer. The internal oxide particles are also rich in Al.

Using these data, a qualitative picture for the oxidation of this group of alloys can be constructed. The first step of the oxidation process appears to be the formation of a NiO layer. The formation of NiO enriches the Al content in areas adjacent to the outer oxide. In alloys with low concentration of Ta and Ti, the enrichment of Al enables the formation of a protective layer of Al_2O_3. On the other hand, in alloys with high concentration of Ta and Ti, a mixture of complex oxides are formed.

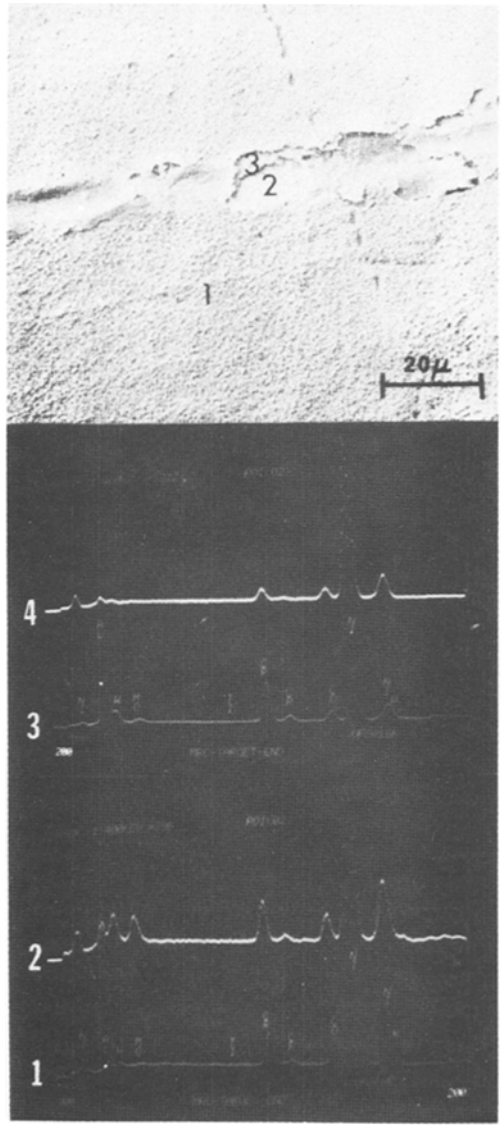

Fig. 8. The scratched surface alloy A oxidized at 1100°C for 60 hr. The EDA spectrum from the marked areas are shown. Spectrum 4 is obtained from Area 1 with point electron source aimed at the center of an oxide crystal.

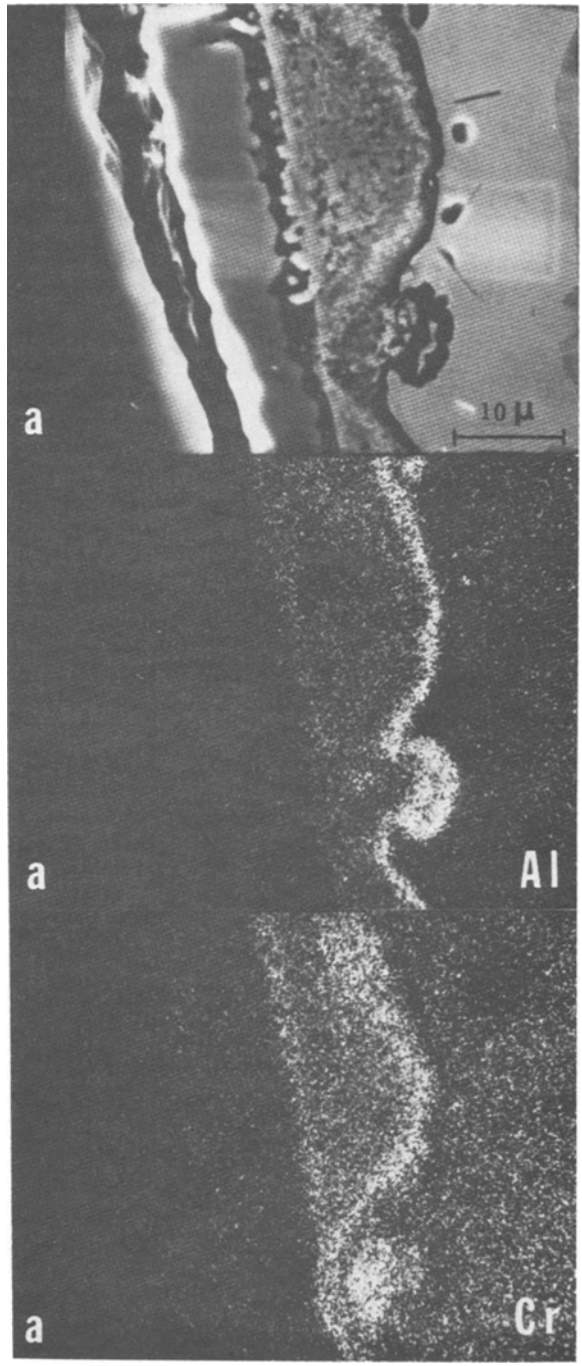

Fig. 9. Alloy A distribution of elements in various layers of oxides. Specimen oxidized at 1100°C for 60 hr.

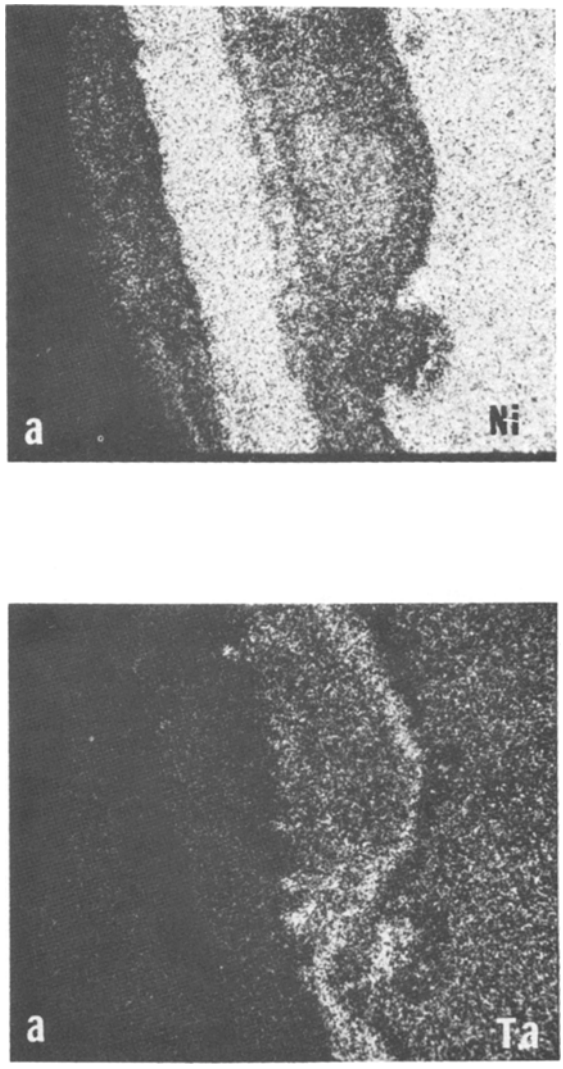

Fig. 9. Continued.

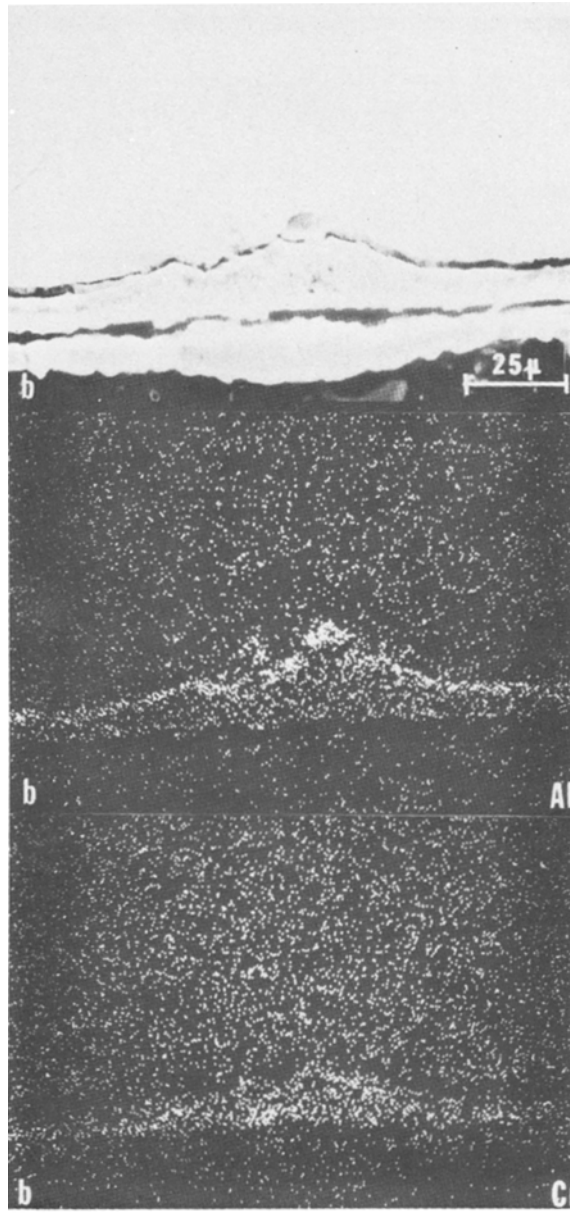

Fig. 10. Alloy B. Distribution of elements in various layers of oxide. Specimen oxidized at 1100°C for 60 hr.

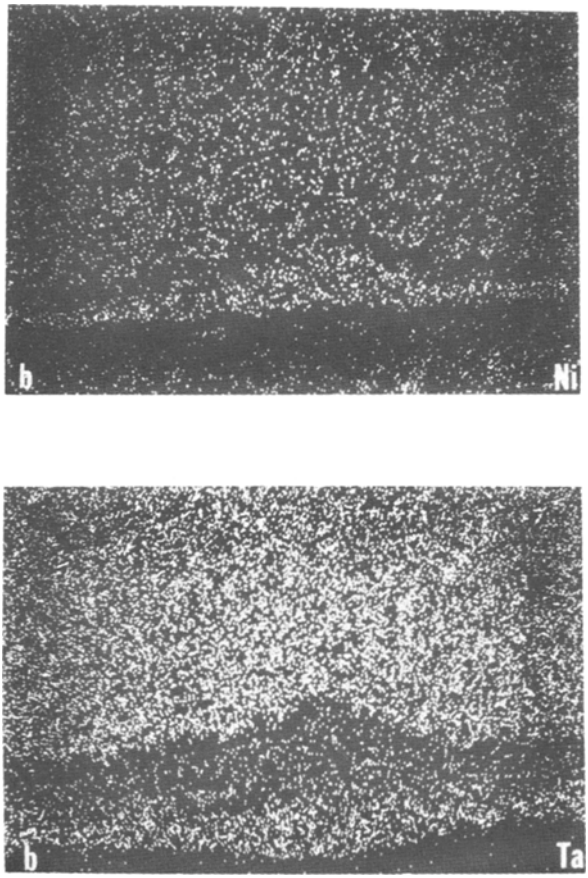

Fig. 10. Continued.

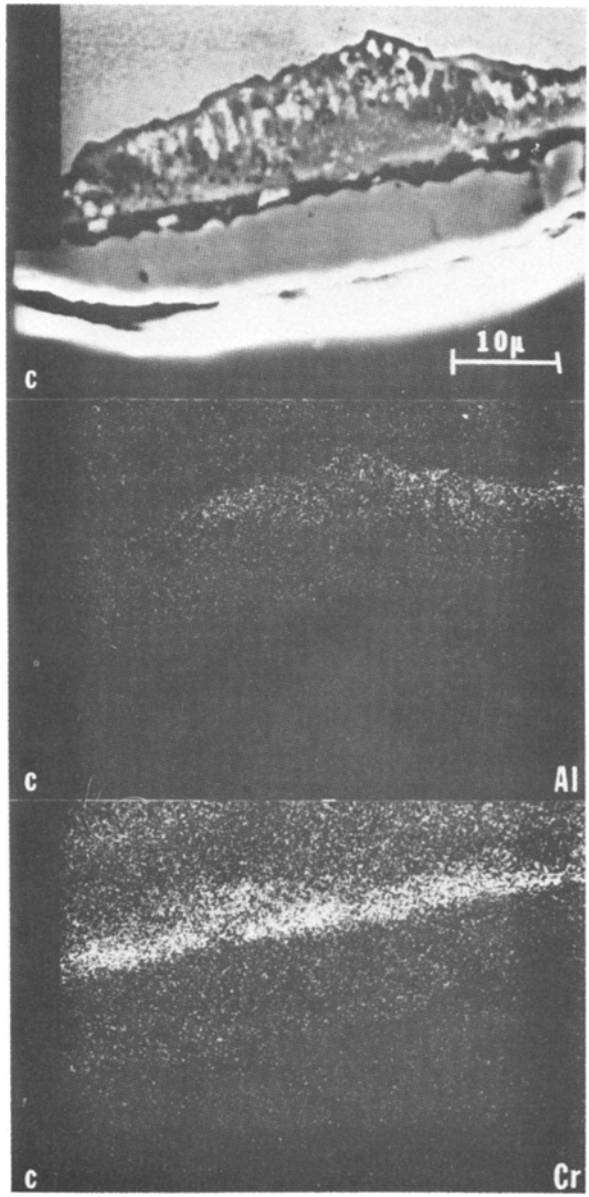

Fig. 11. Alloy C. Distribution of elements in various layers of oxide. Specimen oxidized at 1100°C for 60 hr.

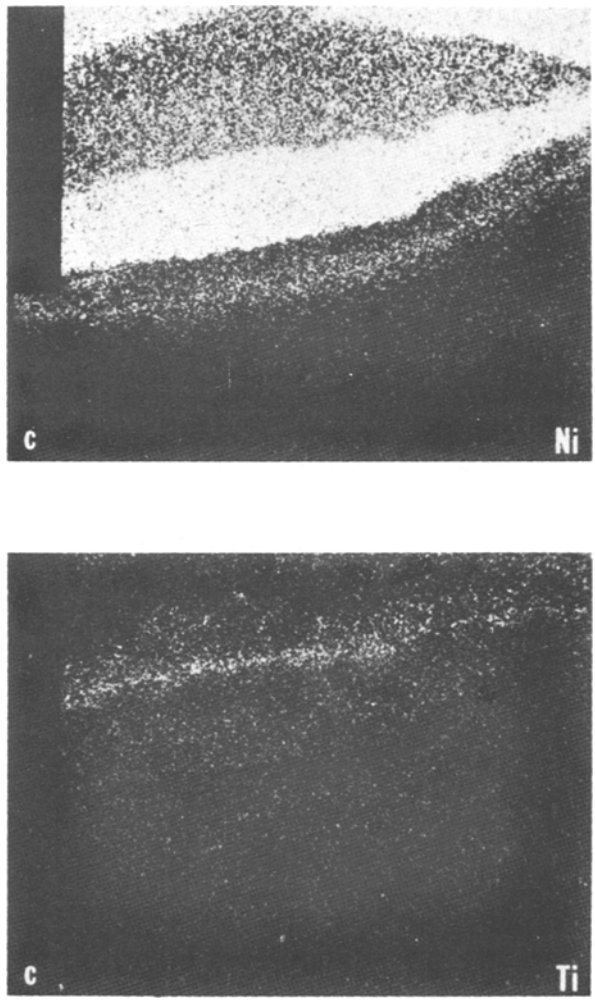

Fig. 11. Continued.

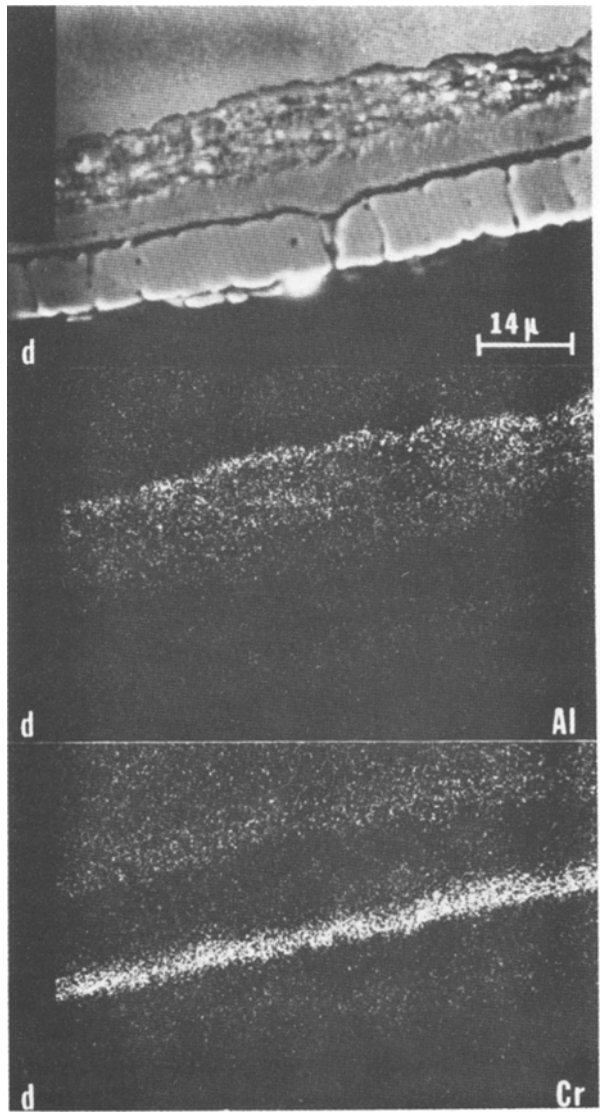

Fig. 12. Alloy D. Distribution of elements in various layers of oxide. Specimen oxidized at 1100°C for 60 hr.

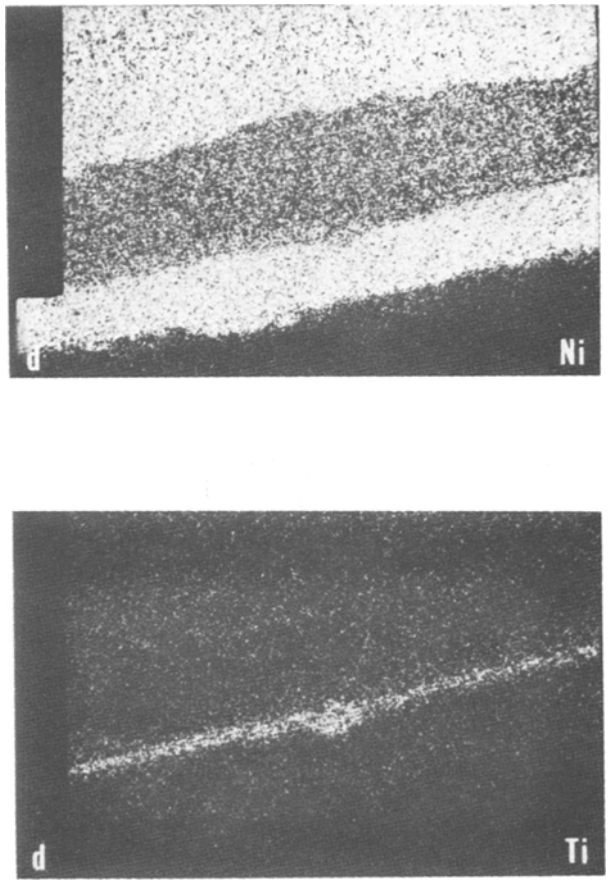

Fig. 12. Continued.

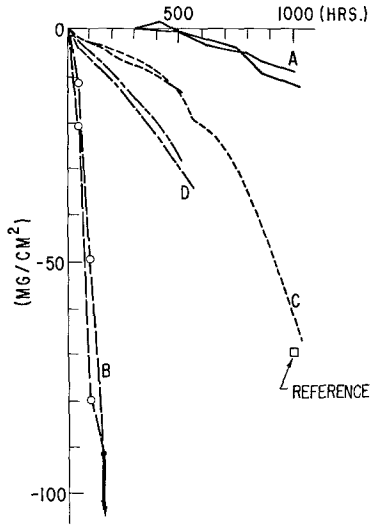

Fig. 13. Weight change during 1100°C cyclic oxidation.

Cyclic Oxidation

Cyclic oxidation of these alloys was chiefly conducted at a furnace temperature of 1100°C. The 1100°C results are shown in Fig. 13. Duplicate tests of shorter duration were performed to assess scatter in the data. Cyclic oxidation using a 1000°C furnace temperature were also performed. The 1000°C results after 500 cycles are listed in Table III. Under the two furnace temperatures, the alloys A and C perform better than the others. The 1000°C cyclic oxidation tests were in general agreement with those conducted at 1100°C. These were also reflected by the oxides present in the scale.

DISCUSSION

The isothermal oxidation kinetics of this group of alloys shown an initial fast weight gain, followed by an extensive period of very slow weight gain.

Table III. Weight Change After 500 Cycles Between 1000°C and Room Temperature

	Alloy, w(mg/cm^2)			
	A	B	C	D
Test 1	+0.07	−4.84	−0.56	−0.71
Test 2	−0.05	−3.10	−0.67	−1.40

The attempt to fit a parabolic rate equation to the experimental data yielded a very poor correlation. The kinetics resemble that of the γ'-δ eutectic alloy[8] but at a slower rate. Disregarding those kinetic curves which involve isothermal spallation (alloys B and D), better correlations with a parabolic rate equation were obtained. The data shows that alloy A oxidized at the slowest rate. This is consistent with the results of cyclic oxidation tests where alloy A had the least amount of weight loss. Agreement can also be found by comparing the sectional micrographs of Figs. 7a and 7c. It is evident that the γ' depleted zone is deeper for alloy C, indicating a faster diffusion of Al atoms. The limited data available indicated that the base alloy had an essentially identical oxidation behavior with that of alloy C under isothermal and cyclic conditions. It appears that 1 at.% Ti does little to alter the oxidation resistance of the base alloy. However, replacing Ti with 1 at.% Ta increases the oxidation resistance considerably. This improved oxidation resistance is manifested by a smaller amount of weight loss under cyclic test conditions.

Both alloys A and C form a protective scale of Al_2O_3, in addition to NiO. The kinetics of oxidation, however, are different for the two alloys. The depth of γ' depleted zones also confirms the difference in the kinetics between the two alloys. If the isothermal kinetic curves are forced to fit an equation of the form:

$$W = Ct + k^{1/2}t^{1/2}$$

the parabolic rate constant, k, can be estimated for alloys A and C. These are tabulated in Table IV. A linear term is included in the equation to account for the volatilization of oxide and possible drift in the electronic system. In each case, the linear coefficient is 2 orders of magnitude smaller than that of the parabolic term.

The composition of alloy C has an Al–Cr ratio slightly higher that MAR–M200.[9] The parabolic rate constant of alloy C is similar to MAR–M200 at 1100°C, but is faster than MAR–M200 at 1000°C.[4] The parabolic rate constants for alloy A, however, are much lower than those of the commercial superalloys such as MAR–M200 and IN713. In fact, the

Table IV. Parabolic Rate Constant of Alloys A and C[a]

	Temperature, °C	
Alloy	1000	1100
A	1.6×10^{-13}	2.4×10^{-12}
C	1.1×10^{-11}	2.1×10^{-11}

[a] In g^2/cm^4 sec.

magnitude of the rate constants resemble those of Ni–Al–Cr alloys with high Al content, or group III alloys, according to Giggins and Pettit.[3] It was noted that the group III alloys formed a single layer of Al_2O_3 without the NiO outer layer. Alloy A, however, formed NiO, spinel, and Al_2O_3 after prolonged oxidation. Since the kinetics resembled the growth of single Al_2O_3 layer, a protective layer of Al_2O_3 must be established very early during the oxidation and become rate limiting. It is, however, not clear whether the addition of 1 at.% Ta has also modified the mechanical or physical properties of Al_2O_3 which may also impact the oxidation resistance.

Increasing the Ta content to 3 at.% leads to the formation of Ta_2O_5 in alloy B, which was less protective. Moreover, increased Ti and Ta also made the formation of Al_2O_3 less favorable, as shown by Table II. Alloys B and D, therefore, perform poorly under cyclic conditions. The correlation between the data of the cyclic test and that of the isothermal test are not definitive due to the isothermal spalling. It is generally believed that a faster isothermal oxidation leads to a thicker scale and higher growth stress.[10] Since higher growth stress results in earlier spalling, the isothermal test can normally be correlated with the cyclic test. This is not necessarily true when the kinetic curves are not truly representative of the oxidation kinetics of the alloys. No attempt was made to calculate the rate constant for alloys B and D due to the spallation detected early during the oxidation.

In the first hour of oxidation at 1100°C alloys A and B initially form NiO and $NiTa_2O_6$, while alloys C and D form NiO and $NiTiO_3$. Understandably, all the oxides are heavily doped with the metallic elements present in the alloys. As oxidation continued, alloys A and C developed a protective layer of Al_2O_3 with decomposition of $NiTa_2O_6$ and $NiTiO_3$. The kinetics suggests that the Al_2O_3 layer was established earlier in Alloy A. Raising the content of Ta and Ti appears to have upset the stability of Al_2O_3 and the alloys lose their oxidation resistance. The degradation is more severe with higher Ta addition than that with higher Ti content.

The results of this work show that the effects of Ti and Ta are different even though the two elements have similar partitioning behavior in the alloy. The oxidation behavior of the alloys is not solely determined by their Cr and Al contents. It would appear that similar investigations of the roles of other refractory elements could be fruitful in identifying improved superalloy composition.

SUMMARY AND CONCLUSION

The effect of Ta and Ti on oxidation resistance of a complex Ni–base superalloy has been studied. Both isothermal and cyclic oxidation were investigated in a base alloy and in alloys with 1 and 3 at.% Ti or Ta additions.

Both Ti and Ta additions at the 3-at.% level were determined to oxidation resistance. Additions of 1-at.% Ti did not markedly alter the oxidation resistance of the base alloy. However, additions of 1 at.% Ta to the base alloy significantly improved oxidation resistance. This improvement is associated with early establishment of an Al_2O_3 scale.

REFERENCES

1. F. S. Pettit, *Trans. Metall. Soc. AIME* **239**, 1296 (1967).
2. C. S. Giggins and F. S. Pettit, *Trans. Metall. Soc. AIME* **245**, 2495 (1969).
3. C. S. Giggins and F. S. Pettit, *J. Electrochem. Soc.* **118**, 1782 (1971).
4. G. E. Wasielewski, AFML-TR-67-30 (1967).
5. C. T. Sims and W. C. Hagel, *Superalloys* (Wiley, New York, 1972).
6. M. F. Henry, unpublished research.
7. G. R. Wallwork, *Rep. Prog. Phys.* **39**, No. 410 (1976).
8. J. G. Smeggil and M. D. McConnell, *Oxid. Met.* **8**, 309 (1974).
9. G. R. Leverant and B. H. Kear, *Metall. Trans.* **1**, 491 (1970).
10. J. Stringer, *Corros. Sci.* **10**, 513 (1970).